TiO$_2$/Cu$_2$O all-oxide heterojunction solar cells produced by spray pyrolysis

Michele Pavan [a], Sven Rühle [b,*], Adam Ginsburg [b], David A. Keller [b], Hannah-Noa Barad [b], Paolo M. Sberna [c], Daniela Nunes [a], Rodrigo Martins [a], Assaf Y. Anderson [b], Arie Zaban [b], Elvira Fortunato [a]

[a] Departamento de Ciência dos Materiais, CENIMAT/I3N, Faculdade de Ciências e Tecnologia–Universidade Nova de Lisboa and CEMOP/Uninova, 2829-516 Caparica, Portugal
[b] Department of Chemistry, Center of Nanotechnology & Advanced Materials, Bar Ilan University, Ramat Gan, Israel
[c] MATIS IMM-CNR and Dipartimento di Fisica e Astronomia, Università di Catania, via S. Sofia 64, 95123 Catania, Italy

A R T I C L E   I N F O

A B S T R A C T

Here we present for the first time a TiO$_2$/Cu$_2$O all-oxide heterojunction solar cell entirely produced by spray pyrolysis onto fluorine doped tin oxide (FTO) covered glass substrates, using silver as a back contact. A combinatorial approach was chosen to investigate the impact of the TiO$_2$ window layer and the Cu$_2$O light absorber thicknesses. We observe an open circuit voltage up to 350 mV and a short circuit current density which is strongly dependent of the Cu$_2$O thickness, reaching a maximum of $\sim$0.4 mA/cm^2. Optical investigation reveals that a thickness of 300 nm spray pyrolysis deposited Cu$_2$O is sufficient to absorb most photons with an energy above the symmetry allowed optical transition of 2.5 eV, indicating that the low current densities are caused by strong recombination in the absorber that consists of small Cu$_2$O grains.

© 2014 The Authors. Published by Elsevier B.V. This is an open access article under the CC BY-NC-ND license (http://creativecommons.org/licenses/by-nc-nd/3.0/).

1. Introduction

Metal oxide (MO) semiconductors are promising for photovoltaic applications; many MOs are abundant, non-toxic and chemically stable which allows material deposition under ambient conditions [1]. Today MOs are already widely used as active or passive components in a broad range of available commercial applications such as active channel layer in transistors that constitute the active matrix of displays [2] or in solar cells as transparent conducting front electrodes and as electron or hole transport layers [3]. Heterojunctions entirely based on MOs, so called all-oxide photovoltaic cells, are recently attracting considerable attention due to their promising potential for price reduction using cheap materials and production methods [4–6].

Heterojunction ZnO/Cu$_2$O cells are the best investigated system, [7] where the wide bandgap ZnO acts as a window layer while the Cu$_2$O has a bandgap in the visible region of the sun spectrum at around 2 eV [8]. Even though the Cu$_2$O bandgap is not ideal for sun light (AM1.5G) remarkable light to electric power conversion efficiencies up to 4% have been reported for cells with a ZnO window layer [9] while 5% were reached with a Ga$_2$O$_3$ layer

[10]. An open circuit voltage up to 1.2 V was reported recently for a Ga$_2$O$_3$/Cu$_2$O heterojunction cell [11]. For multi-junction tandem cells with three or more junctions the Cu$_2$O bandgap is nearly optimized [12]. Furthermore, Cu$_2$O is a very attractive absorber for semi-transparent photovoltaics. Besides solar cells, Cu$_2$O thin films have also been used in optoelectronic devices such as thin film transistors [13].

Cu$_2$O is mostly p-type and can be produced by several methods including sputtering, [14] pulsed laser deposition, [15] chemical vapor deposition, [16] electrochemical deposition, [17,18] anodic oxidation, [19] spray pyrolysis, [20] atomic layer deposition, [21] and thermal oxidation of highly pure Cu metal [7,9,10,22,23]. Cu$_2$O based solar cells with a light to electric power conversion efficiency above 4% are mostly based on Cu sheets thermally oxidized at high temperature ($\sim$1000 °C) and very low oxygen partial pressure, leading to a high crystalline quality [7,9,10]. Alternative deposition methods such as electrochemical deposition of a ZnO layer followed by Cu$_2$O has been presented as a low cost fabrication route towards all-oxide photovoltaics, but the resulting devices showed a conversion efficiency of $\sim$1.4% [18,24].

Spray pyrolysis is a very promising low-cost process which can be easily up-scaled for the deposition onto large areas and the process can be carried out at ambient atmosphere, which is a huge advantage over vacuum deposition techniques that require expensive deposition systems. [25] Spray pyrolysis of dense TiO$_2$ layers is

---

* Corresponding author.
  E-mail address: sven.ruhle@gmail.com (S. Rühle).

a well-developed process using an organic precursor solution, which has been widely used to reduce shunting in quantum dot sensitized solar cells [26] and in dye-sensitized solar with a solid state hole conductor [27]. For ZnO it was shown that nano-structures such as rods and wires can be produced by spray pyrolysis [28]. Cu_2O has been produced by spray pyrolysis using an aqueous-alcoholic solution of copper acetate monohydrate as a precursor and glucose as a reducing agent. A reaction mechanism was proposed where the glucose reacts with the copper acetate, reducing the Cu^{2+} cation to metallic copper Cu^0. Subsequently the high temperature permits the oxidation of the metallic copper to Cu_2O [20]. By controlling the temperature and the concentration of the precursor and reducing agent it is possible to obtain only the cuprite phase. Spray pyrolysis deposited Cu_2O was recently applied in a p-type thin film transistor showing how this material can be successfully used in optoelectronic devices [29].

Here we present for the first time a TiO_2/Cu_2O heterojunction solar cells where both MO layers were produced by spray pyrolysis. Spray pyrolysis is a very attractive process for large area fabrication and can potentially be attached to the glass production process such that different layers are sprayed onto a glass substrate while this is still hot. To investigate the spray pyrolysis deposited solar cells in an efficient manner we have applied a combinatorial material science approach [15] to generate combinatorial heterojunction device

libraries with changing TiO_2 and Cu_2O layer thickness. High throughput measurement systems were employed for optical and electrical characterization with the focus to understand the impact of the layer thicknesses on the solar cell performance.

2. Results and discussion

Fig. 1 schematically shows the combinatorial TiO_2/Cu_2O hetero-junction device library approach. FTO covered glass substrates served as a joint front electrode onto which the TiO_2 layer was deposited with a linear thickness gradient parallel to the x-axis (Fig. 1a) followed by the Cu_2O absorber with a linear gradient parallel to the y-axis (Fig. 1b) leading to a total heterojunction thickness profile with a diagonal thickness gradient (Fig. 1c). The left hand side in Fig. 1 shows a schematic representation, while thickness data derived from optical measurements are shown on the right hand side. The TiO_2 thickness was ranging from 60 to 320 nm, while the Cu_2O layer was between 180 to 580 nm thick.

Structural analysis was carried out before deposition of the Ag back contacts by X-ray diffraction measurements (XRD) showing clear peaks of Cu_2O, TiO_2 (anatase) and SnO_2 which originated from the FTO substrate (Supporting Information). SEM images were recorded at different locations of the library corresponding to
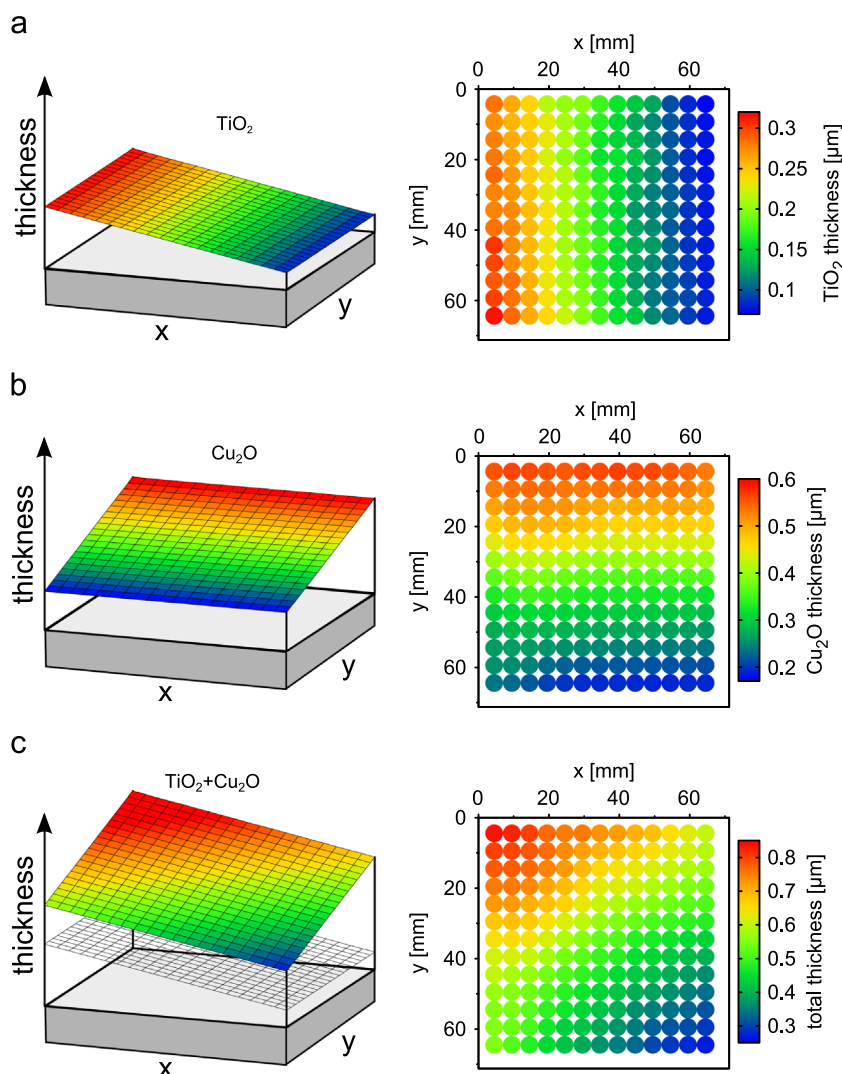

Fig. 1. Schematic representation (left) and measured thickness data (right) of the spray pyrolysis deposited combinatorial device library consisting of FTO layer onto which a) a TiO_2 layer is deposited with a linear gradient in x-direction and b) a linear Cu_2O gradient in y-direction. c) Joint thickness profile of both layers. (For interpretation of the references to color in this figure legend, the reader is referred to the web version of this article.)

different Cu$_2$O thicknesses (Fig. 2). The inset of each Figure shows the Cu$_2$O thickness profile and black points label the location of the SEM measurement. On the top of the library the grain size distribution is homogenous and in the order of 20–50 nm. At slightly thinner Cu$_2$O (Fig. 2b) clusters in the order of 50–100 nm are observed which consist of grains with a very similar size to the one in Fig. 2a. In Fig. 2c the Cu$_2$O crystals have similar size, but without formation of any larger multi-crystalline clusters. At the bottom of the library where the Cu$_2$O is the thinnest one can see again small crystals in a size range like above with some kind of cauliflower morphology. Fig. 2 shows that the crystal size of spray pyrolysis deposited Cu$_2$O is in the order of 20–50 nm, which would correspond to a drop size with a diameter of 0.3–0.7 μm, assuming that each of these crystals grew from an individual droplet during the spray pyrolysis process. The real dropsize in ultrasonnic spray however is in the order of 10 μm and thus significantly larger, indicating that droplets from the spray nozzle decompose into plenty of small droplets when they hit the 300 °C hot substrate surface, which is ~200 °C above the boiling point of the precursor solvents (water and isopronanol). Spray pryolsysis deposited crystals are substantially smaller compared to electro-chemical deposited Cu$_2$O or thermally oxidized Cu$_2$O, which have a grain size in the order of microns to millimeters due to continuous growth of crystallites during material synthesis [7,9,10,30]. EDS maps have been performed after FIB milling experiments (Fig. 2e–h), testing for the homogeneous distribution of Cu, Ti and Sn along the sample. Scattered measurement points outside the layer boundaries are due to the resolution limit of the EDS measurement, namely to the interaction volume of the electron beam with the thin MO films.

Optical transmittance and reflectance measurements were carried out on a grid of 13 × 13 points to determine the optical bandgap. A typical transmittance spectrum of the TiO$_2$/Cu$_2$O heterojunction is shown in Fig. 3a with complete light absorption below ~500 nm, corresponding to an energy of 2.48 eV. This is in good agreement with the bandgap analysis from a Tauc plot, shown in Fig. 3b, where the absorption coefficient α was derived from the total transmission T and reflection spectra R and the absorber thickness d using [31]

$$\alpha(h\nu) = -\frac{1}{d}\log\left(\frac{T(h\nu)}{1-R(h\nu)}\right) \qquad (1)$$

In Tauc plots $(\alpha h\nu)^n$ is plotted versus the photon energy $h\nu$, where $n=2$ for a direct optical transition which is parity allowed. Cu$_2$O has several direct optical transitions, which occur at the Γ-point of the Brillouin zone. For low temperatures (4.2 K) the lowest transitions are reported at 2.17 eV and 2.30 eV, which are both parity forbidden while the first allowed transitions appear at 2.62 eV and 2.76 eV [32]. The band gap is typically temperature dependent and can shrink by some hundred meV at room temperature, thus the derived bandgap for the spray pyrolysis deposited Cu$_2$O layer is in reasonable agreement with the known parity allowed Cu$_2$O transitions from literature. Fig. 3c shows a bandgap map of the full heterojunction library with a bandgap of 2.48 ± 0.03 eV. A bandgap of around 2.49–2.51 eV is observed at the center and top of the library while a slightly smaller bandgap is derived at the bottom of the library. We note that for the derivation of the bandgap from Tauc plots, an automated script was used with the same fitting interval for all spectra. Small
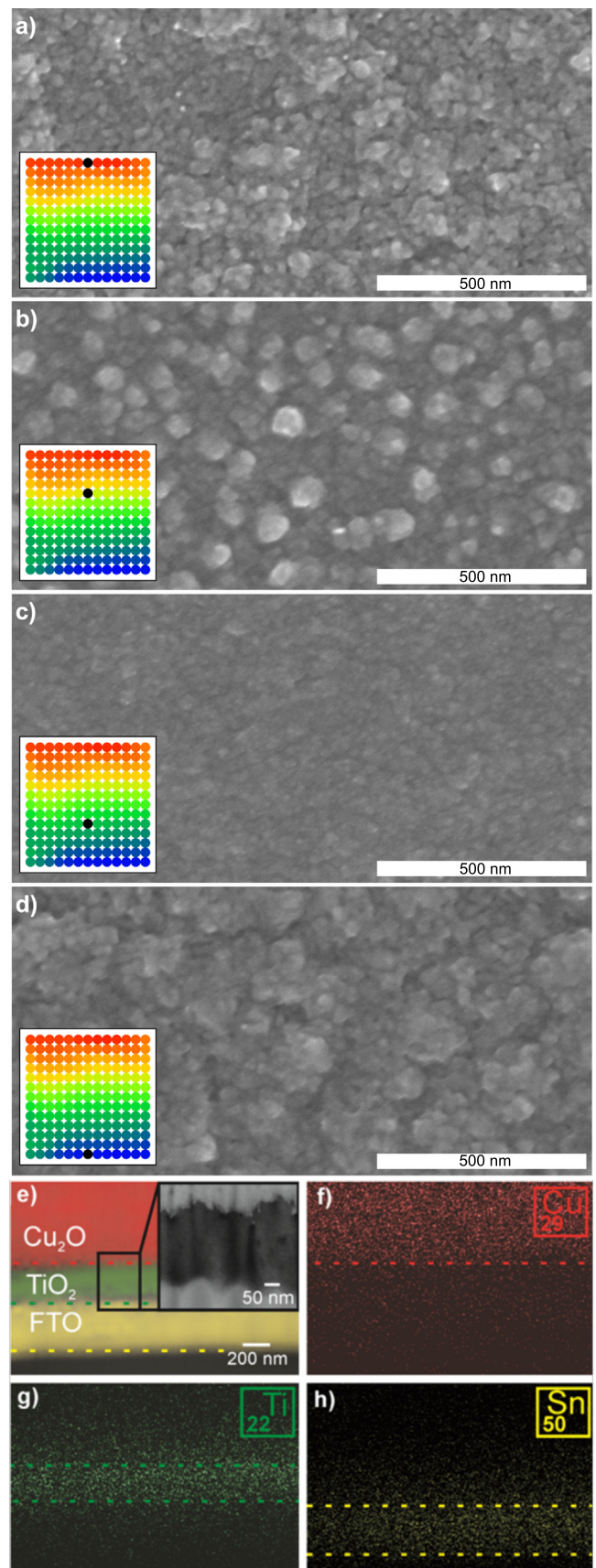

Fig. 2. SEM images of the Cu$_2$O layer at the a) top, b) top-middle, c) bottom-middle and d) bottom of the library. The location of the SEM measurement is shown as a black dot in the inset, which shows the thickness profile of the Cu$_2$O layer. e) SEM image after FIB milling showing in false colors the TiO$_2$/Cu$_2$O heterojunction as well as the FTO layer, and the corresponding X-ray maps in f) Cu, g) Ti and h) Sn. The dashed lines delimitate each individual layer, and the noise is related to the technique constraints. The oxygen map is not presented.

deviations at the bottom of the library might be due to optical interferences within the absorber layer which is only ~200 nm thin in this area. Interferences are not sufficiently taken into account by Eq. (1), leading to a small systematic error of the
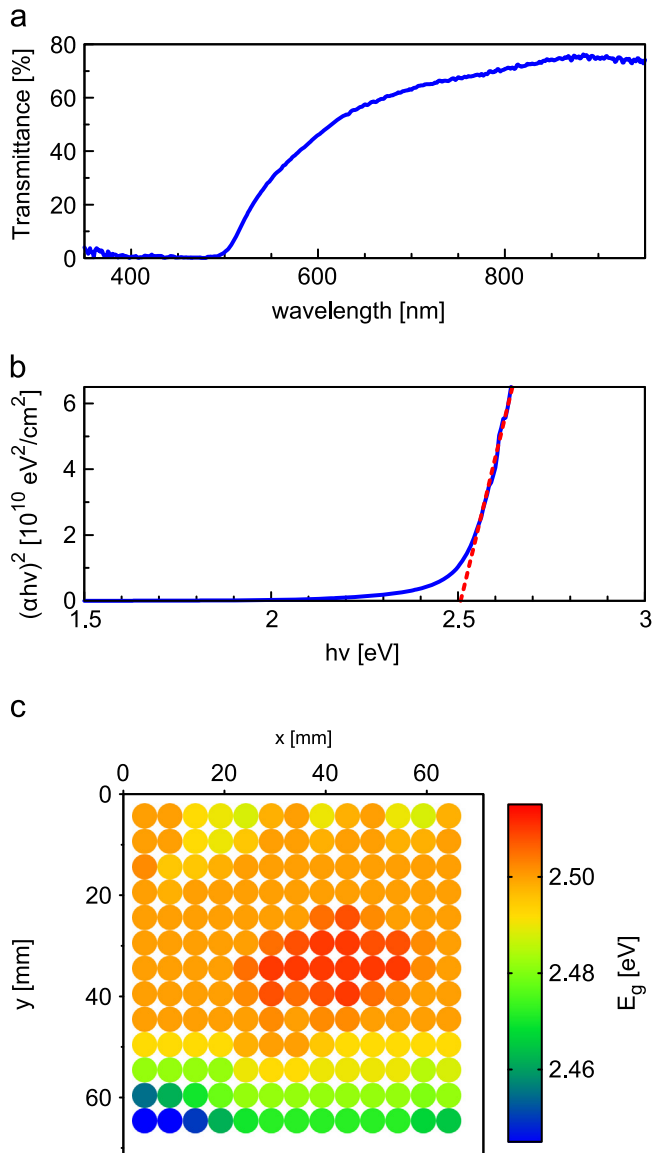
Fig. 3. a) Optical transmittance measured at the center of the device library. b) Typical Tauc plot for a direct allowed optical transition with a linear fit to derive an optical bandgap of 2.5 eV. c) Map of the band gap derived from Tauc plots for the entire library. (For interpretation of the references to color in this figure legend, the reader is referred to the web version of this article).

derivation of α and subsequently of the bandgap derivation for very thin absorber layers.

Light absorption between 2.0 and 2.5 eV is weak due to the symmetry forbidden optical transitions. Tauc plots with an exponent $n=2/3$ have been used by others to derive the bandgap for symmetry forbidden transitions of electrochemical deposited Cu_2O, however for the spray pyrolysis deposited Cu_2O in this work Tauc plots with a 2/3 exponents did not show a linear regime suitable for bandgap derivation. However below we show that even partial light absorption in the range between 2.0 and 2.5 eV has a strong impact on the photocurrent density.

To convert the heterojunction into a solar cell library a grid of 13×13 round Ag back contacts was deposited onto the Cu_2O layer and a metal frame was ultrasonically soldered at the library edges for good electrical contact with the FTO front electrode. A schematic cross-section and top view are shown in Fig. 4a and b, respectively, where the solar cell area was estimated by the size of the back contact, neglecting lateral charge collection from areas surrounding the contact patch. The minimum distance between neighboring cells was 3.2 mm to prevent lateral interaction between neighboring devices. Fig. 4c shows a photograph of the library taken from the glass substrate side with the typical yellow/orange color of Cu_2O. Note that for all maps shown in Fig. 4 the TiO_2 thickness is decreasing from the left to the right while the Cu_2O thickness is decreasing from top to bottom. TiO_2/Cu_2O solar cell libraries in conjunction with automated high throughput characterization systems allow a systematic investigation of the device performance as function of the individual heterojunction layer thicknesses, providing more comprehensive data compared to conventional single device measurements.

I–V scans in the dark and under illumination were performed in each point and three examples are shown in Fig. 4d–f, measured in the points shown in Fig. 4b as dark gray. A higher short circuit current density J_{sc}, and fill factor is observed for the cell with an 550 nm thick Cu_2O layer (4d) while a lower J_{sc} and a poor fill factor are observed for the two examples with thinner Cu_2O (4e,f). Maps of the solar cell parameters J_{sc}, open circuit voltage V_{oc}, fill factor (FF), maximum power density P_{max}, shunt resistance R_{sh} and series resistance R_s all derived from the *I–V* curve under illumination are shown in Fig. 4g–l. Black dots symbolize cells where a substantial difference of the solar parameters was observed depending on the *I–V* scan direction due to hysteresis or cells that did not show photovoltaic action at all.

The highest J_{sc} is achieved when the absorber layer thickness is more than 500 nm. The V_{oc} on the other hand seems to correlate with the total heterojunction thickness with ∼350 mV in the top left corner, where the TiO_2 and the Cu_2O are the thickest, followed by a V_{oc} of ∼300 mV which is observed on the top of the library where the Cu_2O thickness is high or at the left side of the library where the TiO_2 thickness reaches its maximum. A similar trend is observed for the fill factor, with very low values ∼25% that are observed in the lower right half of the library. The maximum electric power density P_{max}, which is the product of J_{sc}, V_{oc} and FF consequently shows a similar pattern like the fill factor, with the highest values on top of the library. Multiplying P_{max} by 100% and dividing it by the incident light intensity of 95 mW/cm² (corresponding to simulated AM1.5G spectrum without photons with a wavelength < 400 nm) leads to the light to electric power conversion efficiency, which remains significantly below 1%. The low fill factor corresponds to an ohmic behavior in the quadrant of photovoltaic action implying that the shunt resistance R_{sh} is low and does not differ significantly from the series resistance R_s, which can also be seen from Fig. 4k and l. From Fig. 4 we can conclude that the thickness of the underlying TiO_2 layer has a positive impact on the photovoltage and fill factor, however the overall fill factor is rather low due to a large R_s and a too low R_{sh}. A high density of interface states at the TiO_2/Cu_2O junction, energetically located in the bandgap of both materials, could be involved in the recombination of electrons from the TiO_2 and holes from the Cu_2O and explain the low R_{sh}.

The photocurrent is strongly increasing with the Cu_2O thickness, which might be an indication for incomplete photon absorption due to an insufficient absorber thickness. To investigate this in more detail we have calculated the maximum photocurrent that can be expected (J_{max}), based on optical transmission and reflection data. Fig. 5a shows a map of J_{max}, calculated according to [33]

$$J_{max} = \int_{\lambda_{onset}}^{\lambda_g} (1 - T(\lambda) - R(\lambda)) \Phi(\lambda) \, d\lambda$$

where $(1 - T(\lambda) - R(\lambda))$ is the fraction of photons that are absorbed and $\Phi(\lambda) \, d\lambda$ is the photonflux in the wavelength interval $d\lambda$ defined by the AM1.5G standard spectrum. For the data in Fig. 5a the integration was carried out from the onset of the solar spectrum in the UV (λ_{onset}) until the band gap (λ_g), taking the
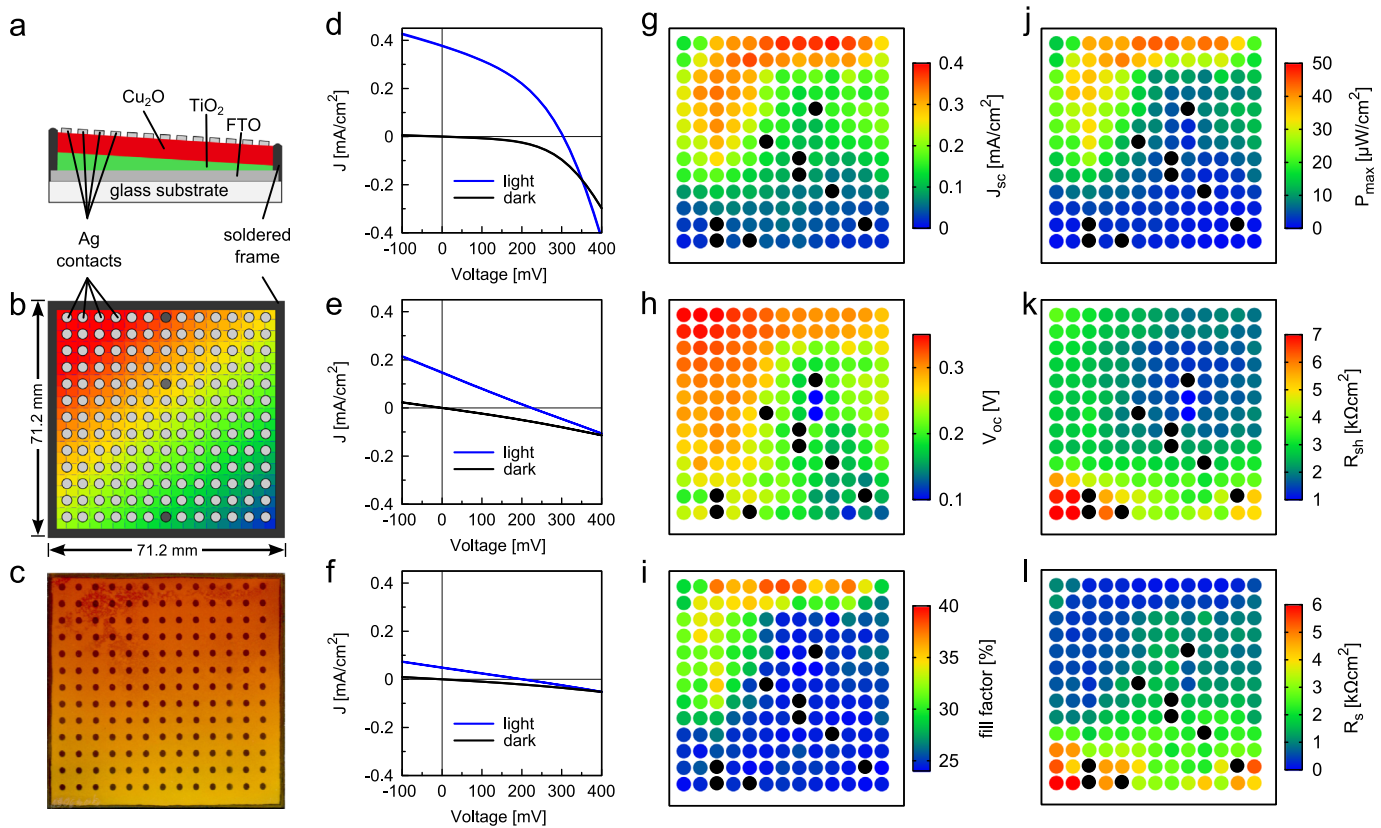
Fig. 4. Combinatorial PV device library: a) cross-section view showing thick TiO_2 on the left hand side and thin TiO_2 on the right hand side. b) Schematic top view of the heterojunction library with the Ag contacts using a color map corresponding to the total heterojunction thickness (TiO_2+Cu_2O). c) Photograph of the library. Dark and light I–V curves measured at the d) top, e) middle and f) bottom of the library (shown by dark gray points in b). Maps of the g) J_{sc}, h) V_{oc}, i) fill factor, j) maximum power output P_{max}, k) shunt resistance R_{sh} and l) series resistance R_s derived from the I–V curve under illumination. (For interpretation of the references to color in this figure legend, the reader is referred to the web version of this article).

bandgap data from Fig. 3c. One can see that the difference in the calculated maximum photocurrent is minor, ranging from 5.0–5.6 mA/cm². Fig. 5b presents the J_{max} as a function of the Cu_2O thickness (blue circles), showing that a thickness of 300 nm is sufficient to absorb most of the photons with an energy above band gap. The green circles show J_{max} when the integration is carried out until $\lambda_g=620$ nm, corresponding to a band gap of 2.0 eV, which is parity forbidden and consequently light absorption is weak. The red circles are the difference between green and the blue circles, thus showing the J_{max} that can be expected due to the weak light absorption between 2.0 and ~2.5 eV. This keeps increasing as a function of the Cu_2O thickness showing that even at the maximum thickness of ~550 nm only a fraction of photons is absorbed, which can be estimated when looking at maximum possible photocurrent $J_{AM1.5G}$ (Fig. 5c). In contrast to J_{max}, where we carry out the integration of the fraction of absorbed photons we assume for the calculation of $J_{AM1.5G}$ that all photons with an energy above bandgap are absorbed and converted into electric current with a quantum efficiency of 100%. One can see that for a band gap of 2.5 eV a maximum current density of 6.27 mA/cm² is possible, which is close to the J_{max} of 5.6 mA/cm² of the presented device library where mainly reflection of the incident light at the air/glass interface accounts for the lower current density. For a band gap of 2 eV a theoretical maximum photocurrent $J_{AM1.5G}$ of 14.7 mA/cm² can be achieved, which is significantly higher than the calculated 9.2 mA/cm² based on transmission and reflection measurements of the 550 nm thick Cu_2O layer. For the symmetry forbidden transition the absorption coefficient α is weak starting at ~2×10^2 cm⁻¹ at 2 eV and is increasing to ~5×10^4 cm⁻¹ at 2.5 eV, [31] thus requiring a larger absorber thickness for that

spectral range. In a photovoltaic device with a bandgap of 2.0 eV approximately 60% of the theoretically achievable current density is due to photon absorption between 2.0 and 2.5 eV and for Cu_2O the absorber thickness has to in the order of microns to absorb most photons in that range.

The measured short circuit current density as a function of the Cu_2O absorber thickness is shown in Fig. 5d. On one hand one can see that J_{sc} is strongly increasing with increasing thickness, which is not observed for J_{max} with its moderate dependence on the Cu_2O thickness. On the other hand J_{sc} remains one to two orders of magnitude below J_{max}, indicating that the spray pyrolysis deposited Cu_2O layer is limited by a low electronic quality, leading to strong recombination rather than insufficient light absorption. The strong thickness dependence of the J_{sc} might be associated to the deposition process in which the absorber is sprayed layer by layer with a successively increasing spray area to achieve a thickness gradient (see also Supporting information). Thus the first layer remains significantly more time on the hot plate than the last layer which might improve the crystallinity at the TiO_2/Cu_2O interface and/or reduce the defect concentration due to slight variations in the Cu/O stoichiometry.

Further investigation of the spray pyrolysis deposition process is required to improve the performance of sprayed Cu_2O hetero-junction solar cells. As pointed out by others, larger Cu_2O crystals of higher quality have to be achieved in order to increase the photocurrent [7]. Furthermore, replacing the TiO_2 electron conducting layer by ZnO or other n-type wide bandgap MOs might improve the conversion efficiency, especially the photovoltage. The TiO_2/Cu_2O junction has a large conduction band discontinuity ΔE_{CB} which leads to a loss in photovoltage (see Fig. 6). In sputtered
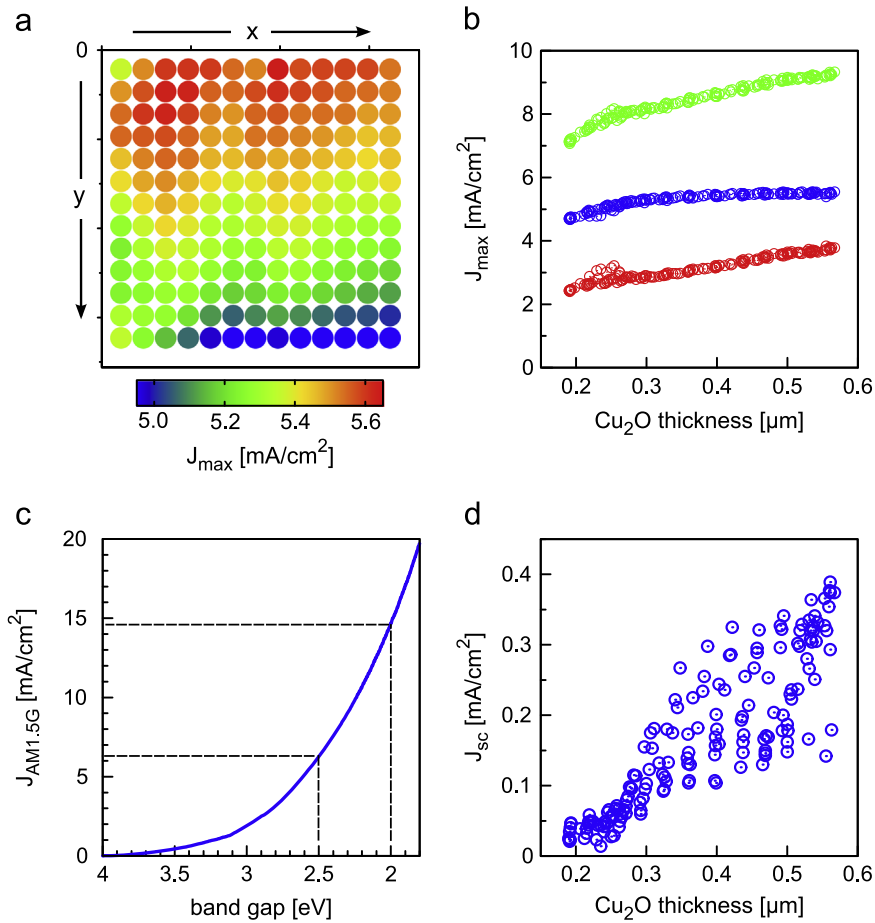
Fig. 5. a) Map of the maximum photocurrent J_{max} that can be expected based on total transmission and reflection data. b) J_{max} as a function of the Cu$_2$O thickness calculated for the symmetry forbidden bandgap of 2 eV (green) and for the symmetry allowed bandgap at ~2.5 eV (blue). The difference of both is shown in red. c) Maximum photocurrent as a function of the band gap energy for the AM 1.5 G spectrum, assuming 100% quantum efficiency for photons with an energy above band gap. d) Measured J_{sc} for the library as a function of Cu$_2$O thickness. (For interpretation of the references to color in this figure legend, the reader is referred to the web version of this article).
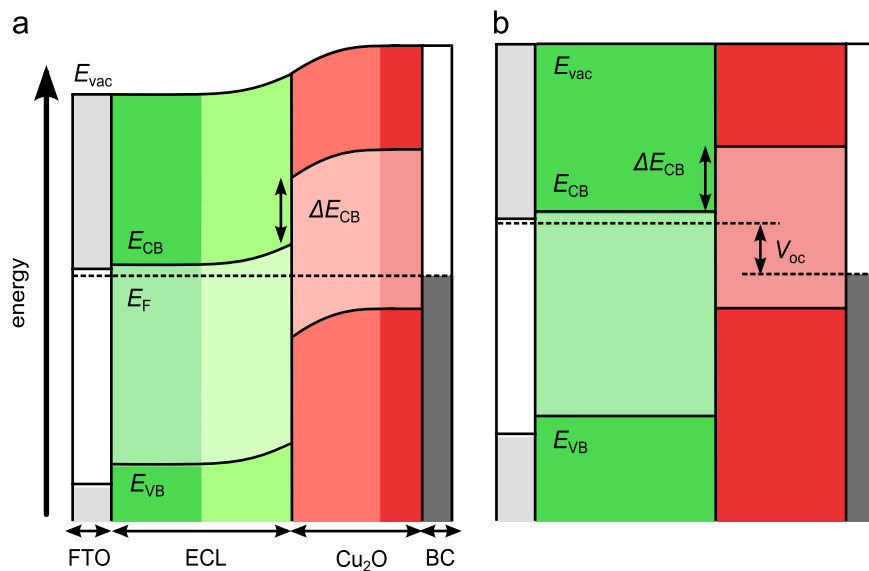

Fig. 6. Energy band diagram of an all oxide heterojunction solar cell at a) short circuit and b) open circuit. A strong conduction band offset at the interface of the electron conducting layer (ECL) and the Cu$_2$O absorber like in TiO$_2$/Cu$_2$O heterojunctions leads to a low V_{oc} compared to the Cu$_2$O band gap.

TiO$_2$/Cu$_2$O junctions it was shown that this discontinuity can reach up to 1.4 eV [34] and work is in progress to investigate this offset at interfaces based on spray pyrolysis produced TiO$_2$ layers. The ZnO/Cu$_2$O heterojunction is an all-oxide photovoltaic heterojunction that has shown promising light to electric power conversion efficiencies with a smaller ΔE_{CB} of 0.97 eV [35] compared to the TiO$_2$/Cu$_2$O junction. A better alignment of the conduction bands is possible by alloying ZnO with Mg, [36–39]

however even for the highest achievable Mg content and staying within the wurtzite crystal structure an offset in the conduction band between $Mg_xZn_{1-x}O$ and Cu_2O of 0.2 eV remains [35]. It was demonstrated that alloy $Mg_xZn_{1-x}O$ with x up to 10% increase the V_{oc} and the efficiency of the solar cells due to the reduction of the conduction band offset; percentage above 10% resulted in decreasing the performance due to the higher resistivity of the obtained compound [36]. $Mg_xZn_{1-x}O$ can also be deposited by SP [40]. A V_{oc} of around 1.2 V was recently reported for a Ga_2O_3 window layer, which has a conduction band edge closer to the vacuum level, thus reducing the conduction band offset at the interface with the Cu_2O absorber [11]. Furthermore, a hole transport layer between the Cu_2O and the metal back contact might be incorporated as well, in order to increase the charge selectivity of the contacts. The low cost technique and the high throughput characterization presented in this work have the potential for a fast development of a low cost optimization.

3. Conclusion

We have presented an all-oxide TiO_2/Cu_2O heterojunction solar cell produced by spray pyrolysis, which is to the best of our knowledge the first time that an entire heterojunction has been produced by this easily up-scalable low cost technique. Using a combinatorial device library approach together with high throughput electrical and optical characterization we have derived a direct bandgap of 2.5 eV with a strong absorption coefficient such that nearly all photons with an energy above 2.5 eV are absorbed within a Cu_2O thickness of 300 nm. Light absorption of the symmetry forbidden bandgap at 2.0 eV is considerable weaker and requires absorber thicknesses in the order of microns. The photocurrent of the spray pyrolysis deposited heterojunction remains with 0.4 mA/cm^2 significantly below maximum photocurrent based on the number of absorbed photons. We attribute this to a small Cu_2O grain size and a high density of grain boundaries that might enhance recombination. To improve the photovoltaic characteristics larger Cu_2O grains of higher quality have to be synthesized and the conduction band offset at the TiO_2/Cu_2O interface has to be reduced.

4. Experimental section

4.1. Spray pyrolysis of TiO_2

Compact TiO_2 layers were deposited by spray pyrolysis in a homebuilt setup. Fluorine doped SnO_2 (FTO) covered glass substrates with a size of 71.2×71.2 mm^2 and a sheet resistance of 15 Ω/square (TEC 15, Hartford Glass Co. Inc.) were thoroughly washed with soap, rinsed with ethanol followed by de-ionized water and were dried in a dry air stream. The substrates were placed onto a Ceran hotplate (Harry Gestigkeit GmbH) heated to 450 °C and a precursor solution of 0.1 M titaniumtetraisopropoxide and 0.1 M acetylacetone in ethanol and isopropanol (mixing ration 1:1) was sprayed with a pneumatic spray nozzle (Spraying Systems Co.) at a rate of 60 cm^3/h, controlled by a syringe pump (Razel Scientific Instruments) while clean compressed air at a flow rate of 6 l/min was used as a carrier gas. The nozzle was mounted onto a commercial x–y scanner (EAS GmbH) using a x–y scan velocity of 30 mm/s and a nozzle - substrate distance of ∼7 cm. A linear thickness gradient was produced using a series of spray cycles with a successively decreasing scan area.

4.2. Spray pyrolysis of Cu_2O

The Cu_2O film was deposited onto the TiO_2 layer using a commercial spraying system (SONOTEK Exacta Coat). A precursor solution of 0.02 M Copper (II) acetate monohydrate ($Cu(CH_3COO)_2H_2O$) and 0.03 M of glucose dissolved in water and isopropanol (mixing ratio 4:1) was sprayed by the ultrasonic nozzle onto the substrate that was maintained at 300 °C using a hot plate. The solution flow rate was 1 mL/min and the airflow pressure was 5.6 bars. The x–y deposition scan velocity was 25 mm/s and the nozzle to substrate distance was approximately 18 cm. A series of spray cycles with a progressive larger scan area was used to produce a linear Cu_2O thickness gradient, orthogonal to the TiO_2 thickness gradient. In order to maintain in each point of the substrate the same condition of reaction and avoid the formation of CuO, the deposition scan program was designed to spray the solution at the same points of the substrate every 50 s. The total sprayed precursor volume was 27 mL.

4.3. Structural characterization

X-ray diffraction (XRD) patterns were obtained using the computer-controlled Panalytical XpertPRO system (Cu Kα radiation; $\lambda = 1.5405$ Å) in Bragg–Brentano geometry ($\theta/2\theta$ coupled). Scanning electron microscopy (SEM) measurements were carried out using a Helios 600 system (FEI) and an AURIGA CrossBeam workstation (Carl Zeiss), both equipped for Energy Dispersive X-Ray Spectroscopy (EDS) analyses. Scanning electron microscopy (SEM) measurements were carried out using a Helios 600 system (FEI) and an AURIGA CrossBeam workstation (Carl Zeiss), both equipped for Energy Dispersive X-Ray Spectroscopy (EDS) analyses. For focused ion beam (FIB) experiments, Ga+ ions were accelerated to 30 kV at 10 pA and the etching depth was kept around 600 nm. EDS maps were carried out after FIB experiments with an accelerating voltage of 15 kV and at a tilt angle of 54° properly indicated on INCA software from Oxford Instruments.

4.4. Optical characterization

Optical transmission and reflectance spectra were measured with a homebuilt scanning system, consisting of a computer controlled x–y scanning table (Märzhäuser Wetzlar GmbH & Co. KG) in conjunction with a specular reflectance probe and two integrating spheres connected by optical fibers to CCD array spectrometers (HR4000, Ocean Optics Inc.) [33]. For total transmittance, total reflectance and specular reflectance measurements the sample was illuminated from the glass substrate side. For total transmittance measurements the light was collected by an integrated sphere from the behind the Cu_2O layer, for total reflectance measurements the integrating sphere was on the side of incident light and specular reflectance was measured with a commercial probe head (Ocean Optics). All measurements were carried out on a grid of 13×13 points after the deposition of each layer for thickness and bandgap analysis as described elsewhere [15].

4.5. Solar cell characterization

For spatially resolved I–V characterization of the heterojunction library a grid of 13×13 Ag back contacts was deposited by thermal evaporation (Vinci Technologies) onto the Cu_2O layer using a shadow mask where each contact patch had a diameter of 1.8 mm, corresponding to an area of ∼0.026 cm^2. Close to the sample edges the sprayed TiO_2 and Cu_2O were mechanically removed using a diamond pen and a frame of soldering alloy was deposited at the substrate edges. I–V characteristics of all 169 devices in the dark and under illumination was measured with a Keithley 2400 source meter in conjunction with automated x–y

scanning table (Märzhäuser Wetzlar GmbH & Co. KG) and a motorized z-stage (Olympus/Märzhäuser Wetzlar GmbH& Co. KG) onto which a gold plated spring loaded tip (Ingun Prüfmittelbau GmbH) was mounted to provide temporary electric contact for measurement of each solar cell. Illumination was provided through a laser pumped Xe lamp (LDLS from Energetics Co.) which was coupled through an optical fiber to the scanning stage. An AM1.5G filter was used to adjust the Xe lamp emission to the sun spectrum and the light was confined to a round spot with a diameter of ~6 mm using a collimating lens.

Acknowledgments

Appendix A. Supporting information

Supplementary data associated with this article can be found in the online version at http://dx.doi.org/10.1016/j.solmat.2014.10.005.

References

[1] R. Jose, T. Velmurugan, R. Seeram, Metal oxides for dye-sensitized solar cells, J. Am. Ceramic Soc. 92 (2009) 289–301.
[2] E. Fortunato, P. Barquinha, R. Martins, Oxide semiconductor thin–film transistors: a review of recent advances, Adv. Mater. 24 (2012) 2945–2986.
[3] E. Fortunato, D. Ginley, H. Hosono, D.C. Paine, Transparent conducting oxides for photovoltaics, MRS Bull. 32 (2007) 242–247.
[4] S. Rühle, A.Y. Anderson, H.N. Barad, B. Kupfer, Y. Bouhadana, E. Rosh-Hodesh, Arie Zaban, All-oxide photovoltaics, J. Phys. Chem. Lett. 3 (2012) 3755–3764.
[5] B.D. Yuhas, P. Yang, Nanowire-based all-oxide solar cells, J. Am. Chem. Soc. 131 (2009) 3756–3761.
[6] J. Morasch, S. Li, J. Brötz, W. Jaegermann, A. Klein, Reactively magnetron sputtered Bi_2O_3 thin films: analysis of structure, optoelectronic, interface, and photovoltaic properties, Phys. Status Solidi A 211 (2014) 93–100.
[7] A. Mittiga, E. Salza, F. Sarto, M. Tucci, R. Vasanthi, Heterojunction solar cell with 2% efficiency based on a Cu_2O substrate, Appl. Phys. Lett. 88 (2006) 163502–163502-2.
[8] L. Olsen, F. Addis, W. Miller, Experimental and theoretical studies of Cu_2O solar cells, Solar cells 7 (1982) 247–279.
[9] Y. Nishi, T. Miyata, T. Minami, Effect of inserting a thin buffer layer on the efficiency in n-ZnO/p-Cu_2O heterojunction solar cells, J. Vac. Sci. Technol. A 30 (2012) 04D103.
[10] T. Minami, Y. Nishi, T. Miyata, High-efficiency Cu_2O-based heterojunction solar cells fabricated using a Ga_2O_3 thin film as n-type layer, Appl. Phys. Express 6 (2013) 044101.
[11] Y.S. Lee, D. Chua, R.E. Brandt, S.C. Siah, J.V. Li, J.P. Mailoa, et al., Atomic layer deposited gallium oxide buffer layer enables 1.2 V open–circuit voltage in cuprous oxide solar cells, Adv. Mater. 26 (2014) 4704–4710.
[12] A.S. Brown, M.A. Green, Detailed balance limit for the series constrained two terminal tandem solar cell, Physica E 14 (2002) 96–100.
[13] E. Fortunato, V. Figueiredo, P. Barquinha, E. Elamurugu, R. Barros, G. Gonçalves, S.-H.K. Park, C.-S. Hwang, R. Martins, Thin-film transistors based on p-type Cu_2O thin films produced at room temperature, Appl. Phys. Lett. 96 (2010) 192102.
[14] J. Deuermeier, J. Gassmann, J. Brötz, A. Klein, Reactive magnetron sputtering of Cu_2O: dependence on oxygen pressure and interface formation with indium tin oxide, J. Appl. Phys. 109 (2011) 113704.
[15] S. Rühle, H.-N. Barad, Y. Bouhadana, D.A. Keller, A. Ginsburg, K. Shimanovich, K. Majhi, R. Lovrincic, A.Y. Anderson, A. Zaban, Combinatorial solar cell

[16] libraries for the investigation of different metal back contacts for TiO_2/Cu_2O hetero-junction solar cells, Phys. Chem. Chem. Phys. 16 (2014) 7066–7073.
[16] S. Eisermann, A. Kronenberger, A. Laufer, J. Bieber, G. Haas, S. Lautenschläger, G. Homm, P.J. Klar, B.K. Meyer, Copper oxide thin films by chemical vapor deposition: synthesis, characterization and electrical properties, Phys. Status Solidi A 209 (2012) 531–536.
[17] J. Cui, U.J. Gibson, A simple two-step electrodeposition of Cu_2O/ZnO nanopillar solar cells, J. Phys. Chem. C 114 (2010) 6408–6412.
[18] S. Jeong, A. Mittiga, E. Salza, A. Masci, S. Passerini, Electrodeposited ZnO/Cu_2O heterojunction solar cells, Electrochim. Acta 53 (2008) 2226–2231.
[19] L. Abrantes, L. Castillo, C. Norman, L. Peter, A photoelectrochemical study of the anodic oxidation of copper in alkaline solution, J. Electroanal. Chem. Interfacial Electrochem. 163 (1984) 209–221.
[20] T. Kosugi, S. Kaneko, Novel spray–pyrolysis deposition of cuprous oxide thin films, J. Am. Ceram. Soc. 81 (1998) 3117–3124.
[21] S.W. Lee, Y.S. Lee, J. Heo, S.C. Siah, D. Chua, R.E. Brandt, S.B. Kim, J.P. Mailoa, T. Buonassisi, R.G. Gordon, Improved Cu_2O-based solar cells using atomic layer deposition to control the Cu oxidation state at the p–n junction, Adv. Energy Mater. 4 (2014).
[22] A. Musa, T. Akomolafe, M. Carter, Production of cuprous oxide, a solar cell material, by thermal oxidation and a study of its physical and electrical properties, Solar Energy Mater. Solar Cells 51 (1998) 305–316.
[23] V. Figueiredo, E. Elangovan, G. Goncalves, P. Barquinha, L. Pereira, N. Franco, E. Alves, R. Marins, E. Fortunato, Effect of post-annealing on the properties of copper oxide thin films obtained from the oxidation of evaporated metallic copper, Appl. Surface Sci. 254 (2008) 3949–3954.
[24] K. Fujimoto, T. Oku, T. Akiyama, Fabrication and characterization of ZnO/Cu_2O solar cells prepared by electrodeposition, Appl. Phys. Express 6 (2013) 086503.
[25] P. Nunes, B. Fernandes, E. Fortunato, P. Vilarinho, R. Martins, Performances presented by zinc oxide thin films deposited by spray pyrolysis, Thin Solid Films 337 (1999) 176–179.
[26] S. Rühle, S. Yahav, S. Greenwald, A. Zaban, Importance of recombination at the TCO/electrolyte interface for high efficiency quantum dot sensitized solar cells, J. Phys. Chem. C 116 (2012) 17473–17478.
[27] U. Bach, D. Lupo, P. Comte, J. Moser, F. Weissörtel, J. Salbeck, H. Spreitzer, M. Grätzel, Solid-state dye-sensitized mesoporous TiO_2 solar cells with high photon-to-electron conversion efficiencies, Nature 395 (1998) 583–585.
[28] M. Krunks, T. Dedova, I. Oja Açik, Spray pyrolysis deposition of zinc oxide nanostructured layers, Thin Solid Films 515 (2006) 1157–1160.
[29] P. Pattanasattayavong, S. Thomas, G. Adamopoulos, M.A. McLachlan T.D. Anthopoulos, P-channel thin-film transistors based on spray-coated Cu_2O films, Appl. Phys. Lett. 102 (2013) 163505.
[30] M. Ichimura, Y. Kato, Fabrication of TiO_2/Cu_2O heterojunction solar cells by electrophoretic deposition and electrodeposition, Mater. Sci. Semicond. Process. 16 (2013) 1538–1541.
[31] C. Malerba, F. Biccari, C. Leonor Azanza Ricardo, M. D'Incau, P. Scardi, A. Mittiga, Absorption coefficient of bulk and thin film Cu_2O, Solar Energy Mater. Solar Cells 95 (2011) 2848–2854.
[32] B. Meyer, A. Polity, D. Reppin, M. Becker, P. Hering, P. Klar, T. Sander, C. Reindl, J. Benz, M. Eickhoff, C. Heiliger, M. Heinemann, J. Bläsing, A. Krost, S. Shokovets, C. Müller, C. Ronning, Binary copper oxide semiconductors: from materials towards devices, Phys. Status Solidi B 249 (2012) 1487–1509.
[33] A.Y. Anderson, Y. Bouhadana, H.-N. Barad, B. Kupfer, E. Rosh-Hodesh, H. Aviv, Y. Tischler, S. Rühle, A. Zaban, Quantum efficiency and bandgap analysis for combinatorial photovoltaics: sorting activity of Cu–O compounds in all-oxide device libraries, ACS Comb. Sci. 16 (2014) 53–65.
[34] L. Huang, F. Peng, F.S. Ohuchi, In situ XPS study of band structures at Cu_2O/TiO_2 heterojunctions interface, Surf. Sci. 603 (2009) 2825–2834.
[35] B. Kramm, A. Laufer, D. Reppin, A. Kronenberger, P. Hering, A. Polity B.K. Meyer, The band alignment of Cu_2O/ZnO and Cu_2O/GaN heterostructures, Appl. Phys. Lett. 100 (2012) 094102.
[36] Z. Duan, A. Du Pasquier, Y. Lu, Y. Xu, E. Garfunkel, Effects of Mg composition on open circuit voltage of $Cu_2O–Mg_xZn_{1-x}O$ heterojunction solar cells, Solar Energy Mater. Solar Cells 96 (2012) 292–297.
[37] T.A. Wassner, B. Laumer, S. Maier, A. Laufer, B.K. Meyer, M. Stutzmann, M. Eickhoff, Optical properties and structural characteristics of ZnMgO grown by plasma assisted molecular beam epitaxy, J. Appl. Phys. 105 (2009) 023505.
[38] S.C. Su, Y.M. Lu, Z.Z. Zhang, C.X. Shan, B.H. Li, D.Z. Shen, B. Yao, J.Y. Zhang D.X. Zhao, X.W. Fan, Valence band offset of $ZnO/Zn_{0.85}Mg_{0.15}O$ heterojunction measured by x-ray photoelectron spectroscopy, Appl. Phys. Lett. 93 (2008) (082108-082108-3).
[39] A. Ohtomo, M. Kawasaki, T. Koida, K. Masubuchi, H. Koinuma, Y. Sakurai, Y. Yoshida, T. Yasuda, Y. Segawa, $Mg_xZn_{1-x}O$ as a II–VI widegap semiconductor alloy, Appl. Phys.Lett. 72 (1998) 2466–2468.
[40] X. Zhang, X.M. Li, T.L. Chen, J.M. Bian, C.Y. Zhang, Structural and optical properties of $Zn_{1-x}Mg_xO$ thin films deposited by ultrasonic spray pyrolysis, Thin Solid Films 492 (2005) 248–252.